Journal Pre-proof

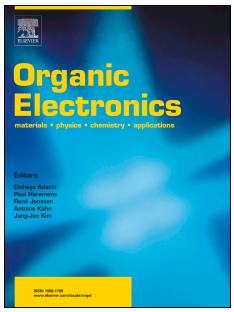

Ultra-low noise PEDOT:PSS electrodes on bacterial cellulose: A sensor to access bioelectrical signals in non-electrogenic cells

Pedro M.C. Inácio, Maria C.R. Medeiros, Tiago Carvalho, Rute C. Félix, Ana Mestre, Peter C. Hubbard, Quirina Ferreira, Jorge Morgado, Ana Charas, Carmen S.R. Freire, Fabio Biscarini, Deborah M. Power, Henrique L. Gomes

PII: S1566-1199(20)30268-8

DOI: https://doi.org/10.1016/j.orgel.2020.105882

Reference: ORGELE 105882

To appear in: *Organic Electronics*

Received Date: 13 March 2020

Revised Date: 12 June 2020

Accepted Date: 21 June 2020

Please cite this article as: P.M.C. Inácio, M.C.R. Medeiros, T. Carvalho, R.C. Félix, A. Mestre, P.C. Hubbard, Q. Ferreira, J. Morgado, A. Charas, C.S.R. Freire, F. Biscarini, D.M. Power, H.L. Gomes, Ultra-low noise PEDOT:PSS electrodes on bacterial cellulose: A sensor to access bioelectrical signals in non-electrogenic cells, *Organic Electronics* (2020), doi: https://doi.org/10.1016/j.orgel.2020.105882.

Author contributions

HLG conceived, planned and coordinated the experiments. PMCI, ALGM and RCF prepared the experiments and performed the electrophysiology. PMCI automated the electrophysiology recordings and wrote the software for the data analysis. TC and CSRF prepared the bacterial cellulose substrates. QF performed the AFM analysis. PCH provided the zebrafish hearts.
MCRM, PMCI and HLG performed electrophysiological data processing and analyzed the electrophysiological data. HLG, RF, DMP, FB, JM, AC and MCRM analyzed and critically discussed the data. MCRM, DMP, PMCI and HLG drafted the manuscript. RCF, MCRM, ALGM, JM, FB, PCH, AC, QF, CSRF, TC, PCH and PMCI critically reviewed the MS contents.

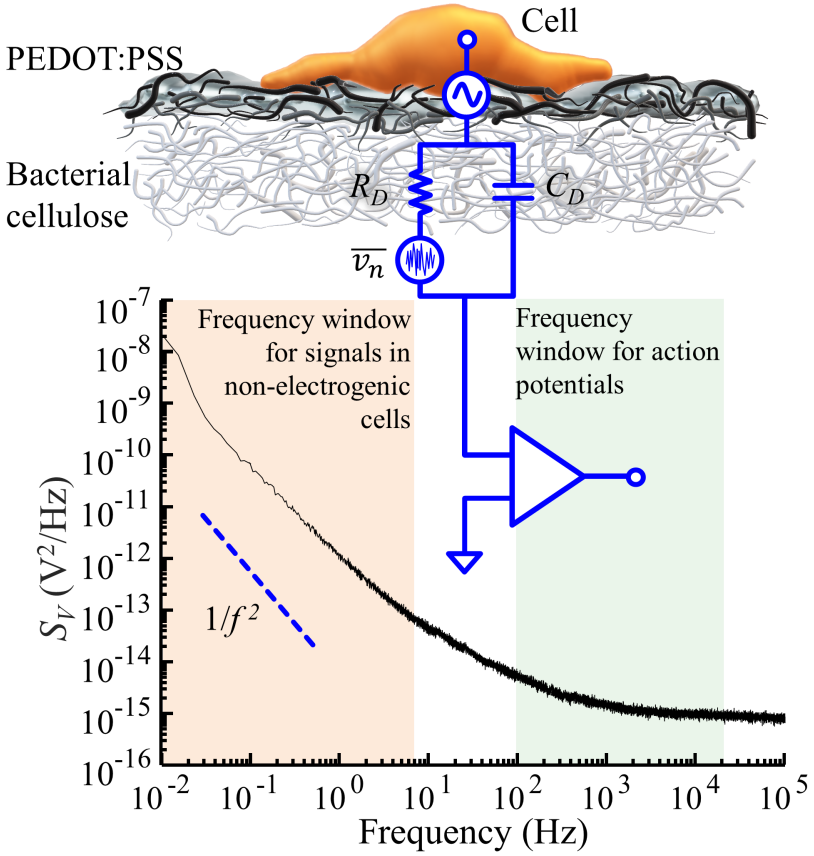
Cell
PEDOT:PSS
Bacterial cellulose
R_D
C_D
$\overline{v_n}$
Frequency window for signals in non-electrogenic cells
Frequency window for action potentials
$1/f^2$
S_V (V²/Hz)
Frequency (Hz)

Ultra-low noise PEDOT:PSS electrodes on bacterial cellulose: a sensor to access bioelectrical signals in non-electrogenic cells

Pedro M.C. Inácio[1,2]†, Maria C. R. Medeiros[3], Tiago Carvalho[4], Rute C. Félix[1,5], Ana Mestre[1,2], Peter C. Hubbard[5], Quirina Ferreira[2], Jorge Morgado[2,6], Ana Charas[2], Carmen S. R. Freire[4], Fabio Biscarini[7,8], Deborah M. Power[1,5] and Henrique L. Gomes[*1,2]

[1]Universidade do Algarve, Faculdade de Ciências e Tecnologia, 8005-139 Faro, Portugal.
[2]Instituto de Telecomunicações, Avenida Rovisco Pais, 1, 1049-001 Lisboa, Portugal.
[3]Instituto de Telecomunicações, Departamento de Engenharia Electrotécnica e Computadores, Universidade de Coimbra, 3030-290 Coimbra, Portugal.
[4]CICECO - Aveiro Institute of Materials, Department of Chemistry, University of Aveiro, 3810-193 Aveiro, Portugal.
[5]Centro de Ciências do Mar, Universidade do Algarve, 8005-139 Faro, Portugal.
[6]Department of Bioengineering, Instituto Superior Técnico, University of Lisbon, Avenida Rovisco-Pais, 1, 1049-001 Lisboa, Portugal.
[7]Dipartimento di Scienze della Vita - Università di Modena e Reggio Emilia, Via Campi 103, 41125 Modena, Italy.
[8]Center for Translational Neurophysiology - Istituto Italiano di Tecnologia, Via Fossato di Mortara 17-19, 44100 Ferrara, Italy.

Abstract

This study is focused on the particular advantages of organic-based devices to measure cells that do not generate action potentials, also known as non-electrogenic cells. While there is a vast literature about the application of organic conductors to measure neurons, cardiomyocytes and brain tissues, electrical measurements of non-electrogenic cells are rare. This is because non-electrogenic cells generate weak signals with frequencies below 1 Hz. Designing low noise devices in a millihertz frequency range is extremely challenging due to the intrinsic thermal and 1/*f* type noise generated by the sensing electrode. Here, we demonstrate that the coating of cellulose nanofibers with conducting PEDOT:PSS ink allows the fabrication of a nanostructured surface that establishes a low electrical double-layer resistance with liquid solutions. The low interfacial resistance combined with the large effective sensing area of PEDOT:PSS electrodes minimizes the thermal noise and lowers the amplitude detection limit of the sensor. The electrode noise decreases with frequency from 548 nV r.m.s at 0.1 Hz to a minimum of 6 nV r.m.s for frequencies higher than 100 Hz. This low noise makes it possible to measure low frequency bioelectrical communication signals, typical of non-electrogenic cells, that have until now been difficult to explore using metallic-based microelectrode arrays. The performance of the PEDOT:PSS-based electrodes is demonstrated by recording signals generated by populations of glioma cells with a signal-to-noise ratio as high as 140.

* Correspondence to: hgomes@ualg.pt

† Present affiliation: Center of electronics optoelectronics and telecommunications (CEOT), Universidade do Algarve.

Keywords: PEDOT:PSS, Printed electronics, Bacterial cellulose, Extra-cellular electrodes, Non-excitable cells.

1- Introduction

Organic conductors and semiconductors are widely accepted as ideal materials to develop the next generation of electrophysiological sensing devices [1–4]. Organic-based electronics possesses the desired mechanical compliance with soft matter and elicit signals with a better signal-to-noise ratio (SNR) than conventional metallic electrodes [5–10]. A number of studies in the literature have demonstrated the superior performance of organic semiconductors when incorporated into structures, such as simple electrodes or transistors [11], to record bioelectrical signals from electrogenic cells, like neurons [6,12,13] and cardiomyocytes [14–16] and even for in vivo recordings [17,18].

The good electrical performance of organic-based devices is part due to the low interfacial impedance, when in contact with liquids. Organic conducting polymers, and in particular, poly(3,4-ethylenedioxythiophene):polystyrene sulfonate (PEDOT:PSS), have an extremely high capacitance. Rivnay et al.[19] showed for the first time the intriguing feature that the capacitance in PEDOT:PSS films scales with their thickness and introduced the concept of volumetric capacitance [20].

The origin of the high capacitive behavior has been also addressed by Volkov et al.[21] who related the high capacitance with the polymer morphology. The authors based their arguments on the fact that as PEDOT:PSS consists on a two-phase structure, formed by hole-conducting PEDOT-rich grains and ion-conducting PSS-rich grains, the capacitance originates from electrical double layers formed along the interfaces between nano-scale PEDOT-rich and PSS-rich interconnected grains.

While the capacitance of PEDOT:PSS electrodes with electrolyte solutions has been well-documented, the corresponding parallel interfacial resistance, often also named charge transfer resistance or ionic resistance of the double layer, has not received so much attention, probably because scientists in this area have focused on recording action potentials. Action potentials generated by neurons or cardiac cells are fast varying signals occurring in milliseconds; their low impedance path is the interfacial capacitor. The corresponding parallel resistance is a high impedance path for alternate (ac) signals and essentially only contributes to sensor thermal noise. Nonetheless, it is desirable to have a relatively low resistance because it improves the signal-to-noise ratio.

When recording signals generated by non-electrogenic cells, the low frequency (f<1 Hz) noise is of utmost importance. For frequencies below 1 Hz, both the thermal noise and the 1/f noise, also known as pink noise [22], combine to increase the noise of the sensing electrode. This problem is aggravated by the low amplitude of the non-electrogenic cell signals, typically below 10 μV.

In biology, low frequency signals are particularly relevant because there is an enormous variety of cell-cell communication mechanisms that use extremely low frequency (f<mHz) signals. For example, cancer cells use low frequency signals to proliferate, migrate and synchronize their activity [23,24]. Recently, the measurement of bioelectrical signals generated by non-electrogenic cells has started to attract attention. Using gold-based electrodes, we previously reported the recording of these low frequency signals in astrocyte populations and in glioma cells [25–28], and others have also reported the recording of signals in prostate cancer cells [29] using similar electrodes. Other approaches have used organic-based transistors to stimulate astrocytes [30] and silver nanowires to record astrocyte signals [31]. However, the detection of these low frequency cellular signals with a good signal-to-noise ratio relies on the use of very large sensing areas (cm^2 range). This strategy has two severe handicaps: firstly, there is a total lack of spatial resolution and, secondly, the co-occurrence of many uncorrelated signals results in an overall signal that resembles noise.

In this study, we propose that organic-based devices, due to their low interfacial resistance with liquids, offer a disruptive technology to access an important class of low frequency bioelectrical communications in non-electrogenic cells. The low interfacial resistance of organic devices has two important roles that are presented and discussed. First, the low resistance minimizes the thermal noise and, second, provides a low impedance path for slow varying or long-lasting signals. This steady-state component of the signal contributes to increase the recorded signal strength, therefore increasing the SNR.

With the perspective of taking full advantage of the electronic properties of the organic thin films, we deposited PEDOT:PSS on bacterial cellulose (BC) substrates. BC is a biomaterial produced by some non-pathogenic bacteria in the form of wet membranes [32]. In comparison with plant cellulose, BC has several advantages such as high purity, superior water uptake capacity and mechanical robustness. In the

context of PEDOT:PSS-based electrophysiological devices, BC offers a number of crucial advantages. Particularly relevant is the good adhesion of PEDOT:PSS to the BC substrates. PEDOT:PSS does not delaminate from BC substrates, as often occurs in flat substrates, such as glass. In addition, BC has a peculiar 3D porous structure composed of nano- and micro-fibrils [32] whose micro-roughness provides an enhanced active area to contact with cells. Further, such microarchitecture and porosity can be adjusted by controlling the bacteria fermentation process [33]. The high affinity for water results in hydrogel-like properties, which are ideal to host cells. In addition, BC is approved by United States Food and Drug Administration (FDA) to be used in biomedical devices [34] and it has been explored in tissue engineering [35], wound healing [36,37], and drug delivery [38–43] among others. However, to the best of our knowledge, the use of BC membranes has never been addressed for electrophysiological-based devices.

The basic concepts of the interfacial electrical double-layer and the role of each impedance component (capacitance and resistance) on the recorded signal shape and thermal noise is presented. Then, the low frequency impedance of PEDOT:PSS deposited either on glass or on bacterial cellulose (BC) is compared with a gold electrode. The thermal noise of the different sensing surfaces is compared to establish the detection limit of each type of electrode. The well-characterized beating of a zebrafish heart is used to benchmark the relative performance of each of the sensing surfaces being analyzed. The optimized sensor using PEDOT:PSS on bacterial cellulose is then applied to record oscillations in glioma cells. Finally, the advantages of using PEDOT:PSS-based electrodes in low frequency electrophysiology studies are discussed.

2- Material and methods

Fabrication of nanofibrous bacterial cellulose

Bacterial cellulose membranes were produced by *Gluconacetobacter sacchari* strain, in Hestrin and Schramm (HS) medium, using glucose as carbon source [44]. In more detail, flasks with the *G. sacchari* bacteria were kept in static conditions, at 30 ºC, for 96 hours. After that period, the membranes were removed and treated three times with 0.5 M of sodium hydroxide, at 90 ºC, for 30 minutes. Afterwards, the membranes were purified by washing with distilled water. In order to obtain thin membranes, wet membranes were dried at 40 ºC.

Electrodes

A standard ink-jet printer (DMP-2831, Fujifilm Dimatix Material Printer) was used to print the sensing devices. Poly(3,4-ethylenedioxythiophene):polystyrene sulfonate, also known as PEDOT:PSS, was purchased from AGFA Orgacon^{TM}. The PEDOT:PSS ink was loaded into a proprietary cartridge model (DMC-11610, Fujifilm). Each printed electrode was the result of eight consecutive prints, resulting in 8 layers of PEDOT:PSS, which corresponds to a thickness of approximately 500 nm. The samples were annealed on a hot plate at 60 ºC for 8 hours. After annealing, the films were immersed into ethylene glycol (EG) and then dried in a vacuum oven at 60˚C for 12h.

Gold electrodes were deposited by thermal evaporation trough a shadow mask. The electrodes are approximately 200 nm thick.

The electrode design consisted of parallel fingers with equal dimensions, with a depth (*D*) of 0.5 mm, length (*W*) of 10 mm, and separated by a gap distance (*L*) of 0.5 mm, forming a total printed electrode area of 5 mm^2. Only 2 mm^2 was used for sensing. A photograph of the fabricated electrodes made of gold and PEDOT:PSS on bacterial cellulose and of PEDOT:PSS on a glass slide is shown in Fig.1 (b).

Electrical and atomic force microscopy characterization

The entire electrical system was maintained within a large iron Faraday cage to minimize external interference. The small-signal impedance measurements were carried out using an RCL meter (Fluke PM 6306), within a frequency range 50 Hz–1 MHz, by applying an ac voltage of 50 mV. Electrical noise measurements were performed using low noise voltage and current pre-amplifiers (SR 560, and the SR 570 Stanford Research Systems) configured for single-ended input. The pre-

amplifiers were connected to a dynamic signal analyzer (DSA) (35670A, Agilent). The DSA recorded the output signal of each preamplifier by applying uniform windows with unitary amplitude to the input signal, proceeded by an FFT to determine the spectral signal density (S_n). The output noise for the setup using the SR560 is given by $S_n(f) = (S_v(f) / A_V)^2$, where $S_v(f)$ is the r.m.s noise measured in V/√Hz for a given frequency, and A_V is the gain of the amplifier.

The power spectral density was measured by dividing the full frequency range (10^{-2} - 10^5 Hz) in several shorter ranges. The total smoothed power spectrum was obtained by joining the 15 shorter frequency bands i.e. 6.25 Hz, 12.5 Hz, 25 Hz, 50 Hz, 100 Hz, 200 Hz, 400 Hz, 800 Hz, 1.6 kHz, 3.2 kHz, 6.4 kHz, 12.8 kHz, 25.6 kHz, 51.2 kHz and 102.4 kHz. All frequency spans represent an average of at least 100 continuous recordings.

Due to redox reactions at the electrode-cell interface, DC voltage levels appear at the sensing electrodes. This DC offset causes a differential DC input signal that can saturate a high-gain DC-coupled differential amplifier [45]. The DC offset was removed by adjusting a tuning capacitance using the front-end offset potentiometer of the SR 560 amplifier.

3 or 4 pairs of sensing electrodes for each type of material and substrate were characterized. Although, there is a small variability of the impedance and noise caused by the material processing, there is also variability caused by the mounting of the sample holder. Because it is difficult to discriminate both sources of variability, statistical analysis of electrical measurements was not carried out.

The bacterial cellulose surface was characterized by atomic force microscopy (AFM) using a NanoObserver from Concept Scientific Instruments (CSI). The sample morphology was analyzed in noncontact mode using silicon probes from APPNano with a radius smaller than 10 nm. The obtained images were processed and analyzed using Gwyddion software.

A Students *t*-test was used to evaluate the statistics of the signal-to-noise ratio and to estimate the significance level (p).

Histogram analysis was used to evaluate the recorded burst of ultra-low frequency signals generated by the Rat C6 glioma cells. The histogram uses bin distributed logarithmic in frequency.

Biological material

Rat glioma cells C6 (ATCC® CCL-107™) were cultured in F-12K nutrient medium

supplemented with 15% fetal horse serum, 2.5% fetal bovine serum, and 1% penicillin and streptomycin. The cells were maintained in an aseptic environment at 37 ºC in a CO_2 incubator (Thermo Scientific Midi 40) with a humidified atmosphere and 5% CO_2. The cells were harvested and 50,000 cells were transferred to the sensing device in 400 µL of medium. The cell suspension generated a confluent monolayer of cells that covered the entire device surface.

A zebrafish heart, when kept in a suitable environment, can beat in a reproducible way for a period as long as 8 hours. This is enough time to move the heart to different electrodes and record the corresponding cardiac signal. Three experiments with three different zebrafish hearts were carried-out. However, the data presented here refers to a single heart, the strongest beating one. The dependence of SNR on the electrode material was identical in all hearts tested.

Zebrafish were anesthetized and sacrificed by immersion in water with an overdose of 300 $mg.L^{-1}$ ethyl-3-aminobenzoate methane sulfonate salt (MS222). The hearts from the zebrafish were surgically extracted and placed in Krebs solution (400 µL) at 24 ºC. Under these conditions the hearts kept beating for up to 24 hours. The size of the zebrafish heart is about 1 mm and it beats about twice a second. Fish care and experimentation complied with the national legislation for the use of laboratory animals under a Group-1 license issued by the Veterinary General Directorate of the Ministry of Agriculture, Rural Development and Fisheries of Portugal.

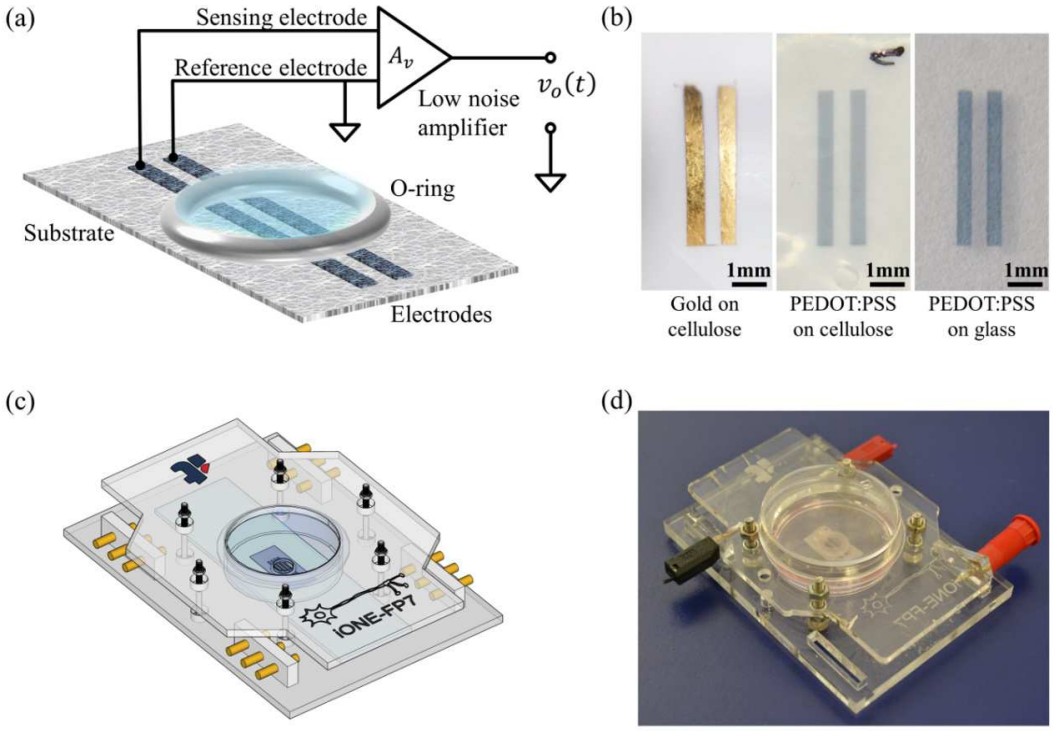

Fig. 1. Electrodes and sample holders. (a) Schematic diagram of the device and the electrical connections to the amplifier. (b) Photographs of the three types of electrodes fabricated. (c) Schematic model of the sensor in the sample holder, (d) Photograph of the fabricated prototype.

3- Results

The goal of this study was to demonstrate the two-fold role of the electrical double-layer (EDL) resistance on the quality of the recorded bioelectrical signal. The results are divided into three parts. The first part is focused on the role of the EDL resistance in minimizing the thermal noise. The electrode performance is demonstrated in the high frequency region (kHz) by measuring the beating of a zebrafish heart. The second part demonstrates the role of the EDL resistance on the shape of the signal. Finally, in the third part, by measuring signals in populations of glioma cells, we demonstrate the performance of the electrodes in the ultra-low frequency region (f<0.1Hz).

3.1- Small signal impedance of the sensing electrodes

We [46] and other authors [16,47–50] have previously described the electrical coupling between cells and sensing electrodes and, for this reason, only a brief summary of the essential features needed to understand the data analysis is provided. The sensing layer is the electrical double-layer (EDL), which, in a simplistic way, is described by an equivalent parallel RC circuit network, as shown in the inset of Fig. 2 (a). EDL is modeled by the parallel network comprised of the double layer capacitance (C_D) and resistance (R_D), also known as charge transfer resistance or ionic resistance of the double layer. The EDL is in series with the bulk electrolyte layer. The bulk electrolyte layer is form by the parallel network comprised by the bulk resistance (R_E) and capacitance (C_E). We include also a series resistance (R_S), due to the electrode. R_S is very small for metallic electrodes but it cannot be neglected when PEDOT:PSS electrodes are used.

The impedance analyzer measures the overall parallel components R_P and C_P. The impedance of the system is strongly frequency dependent. The frequency dependence arises from the fact that C_D is higher than the capacitance of the series bulk electrolyte solution (C_E). The electrode in contact with a liquid behaves as two-layers in series, in addition C_D and R_D are also frequency dependent. Fig. 2 (a) shows the measured parallel capacitance (C_P) and the parallel resistance (R_P) expressed as loss (L_P). $L_P = 1/(2.\pi.f.R_P)$, where f is frequency of the ac probing signal. L_P has a relaxation called the Maxwell-Wagner relaxation [51]. This relaxation occurs at the frequency at which the high interfacial capacitance begins to be short-circuited as the frequency of the signal increases.

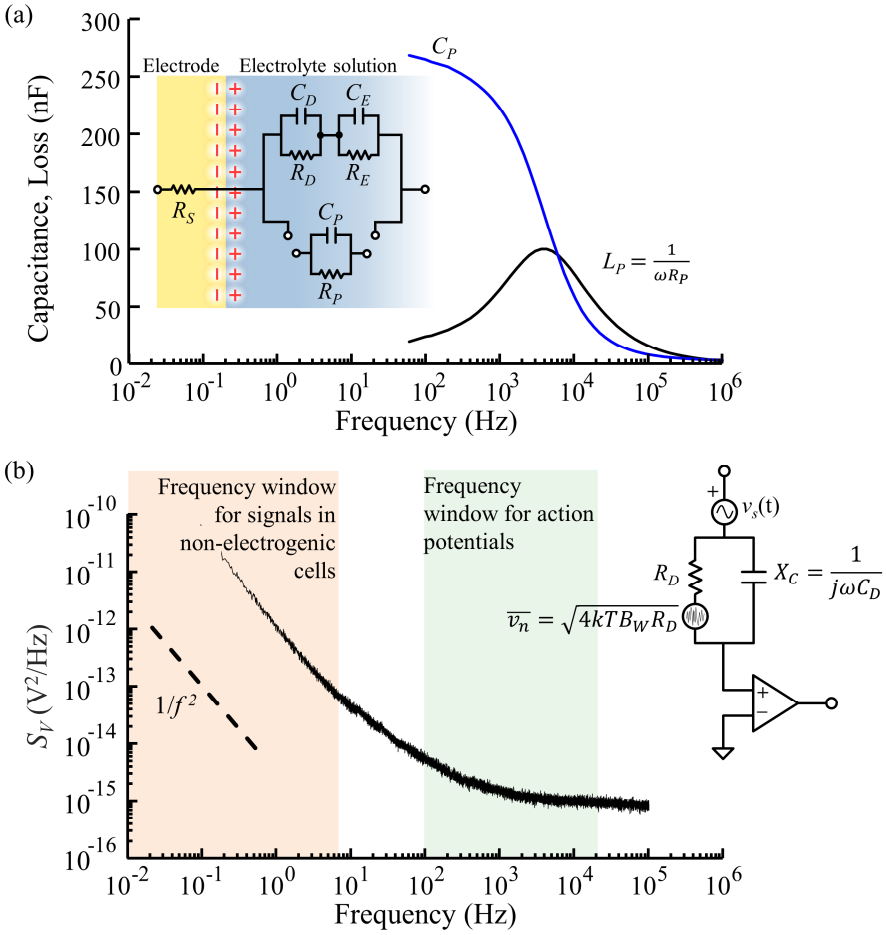

Fig. 2. Electrical double-layers, equivalent circuit and the thermal noise. (a) Frequency response of a gold/electrolyte system in a thermally oxidized silicon substrate. The inset scheme represents the simplified equivalent circuit of the EDL in series with the bulk electrolyte. (b) Noise (S_V) power spectrum density for the electrode with the impedance presented in (a). The inset circuit represents the thermal noise due to R_D.

The power spectral density of the electrical noise in voltage (S_V) measured for the gold/electrolyte interface is shown in Fig. 2 (b). The gold electrode was deposited on a thermally oxidized silicon substrate and the electrolyte was the cell culture medium. The electrode design is presented in Fig. 1 (b). For frequencies below 1 Hz, the noise evolves approximately as $1/f^{\,2}$. This type of noise is known as pink noise and is common in EDLs [52]. In general terms, this type of noise has power spectra following a $1/f^{\,\alpha}$ (with $0.5 \lesssim \alpha \lesssim 1.5$) behavior at low frequencies. It has been observed in a large variety of areas, including, physics, biology and music. However, no general physical explanation of $1/f$ noise has been proposed and its physical origin remains unsolved.

The pink noise in electrode/electrolyte systems was analyzed in detail in a study by Hassid et al. [52]. This reference on the noise of electrode/electrolyte systems shows that in the absence of electrochemical reactions at the electrode interface, the system should only exhibit thermal noise. The observation of excess noise is only expected when charge transfer occurs at the interface. The shape of the noise spectrum depends then on the nature of the charge transfer process: (i) if the mass transfer at the interface is dominated by electric fields, then noise spectra possesses a $1/f$ type dependency; (ii) if the charge relocation is dominated by diffusion, the dependency will be of $1/f^2$ type.

For frequencies above 1 kHz the noise becomes frequency independent (white noise). This noise is caused by thermal noise generated by the resistance associated with the electrode/electrolyte interface. In contrast to the pink noise, thermal noise is well understood and quantitatively explained. The equivalent circuit in the inset of Fig. 2 (b) shows the noiseless resistor (R_D) in series with the corresponding thermal noise source (v_n).

The frequency regions relevant for two types of electrophysiological processes, action potentials and slow oscillations are also highlighted in Fig. 2 (b). The recording of action potentials requires a bandwidth of a few kilohertz (300 Hz - 5 kHz) [53], while bioelectrical oscillations generated by non-electrogenic cells require a frequency window from mHz up to 1 Hz. This milli-hertz spectral region is dominated by pink noise as shown in Fig. 2 (b). When the goal is to develop devices to measure non-electrogenic cells, the lowering of the interfacial resistance is a critical issue. A low interfacial resistance minimizes the intrinsic electrode noise, and PEDOT:PSS-based electrodes on bacterial cellulose substrates offer the lowest interfacial resistance and, therefore, the lowest intrinsic noise. To show that PEDOT:PSS has the performance required to measure non-electrogenic cells, the PEDOT:PSS impedance was compared with the impedance of a metal electrode (gold) and how the morphology of the substrate modifies the impedance of the sensing surface is also demonstrated. The impedance of several electrode/electrolyte interfaces is shown below. The frequency dependence of the parallel capacitance (C_P) is presented in Fig. 3 (a) and the corresponding parallel loss (L_P) in Fig. 3 (b). This individual representation of capacitive and resistive components discriminates better their individual contributions to the impedance of the electrodes and the substrate. In agreement with previous reports, PEDOT:PSS offers a remarkably low impedance when compared with gold

electrodes. Interestingly, the analysis of the individual impedance components, C_P and R_P, reveals that, for frequencies above 1 kHz, the lowering of the impedance is essentially due to a lower interfacial resistance of the PEDOT:PSS electrodes. This low resistance is particularly important for lowering the intrinsic thermal noise.

Fig. 3 (b) compares the loss as function of frequency, for the three electrodes under study. The loss of the PEDOT:PSS measured at the frequency of 60 Hz is approximately 14 times higher than the loss of the gold-based electrode. Since loss is inversely proportional to the resistance, the PEDOT:PSS has 14 times lower resistance that the gold electrode. The difference in resistance between the PEDOT:PSS electrode printed on glass and on cellulose is due to the higher effective surface area of the cellulose nanofibers.

The inset in Fig. 3 (b) shows C_P and L_P in a Cole-Cole representation. In this type of plot, a resistor is simply a dot while an ideal capacitor is a horizontal straight line.

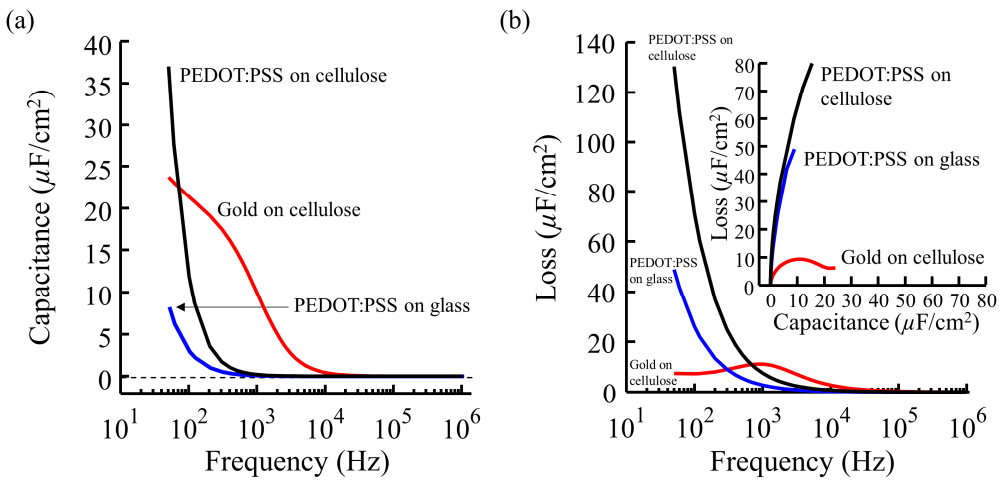

Fig. 3 Comparison between the impedance parameters, capacitance and resistance of printed PEDOT:PSS and gold electrodes on cellulose or glass substrates. (a) Frequency dependence of capacitance (C_P) and in (b) frequency dependence of loss (L_P). The inset shows C_P and L_P in a Cole-Cole representation. All plots were normalized by the total sensing electrode area, A=2 mm^2.

The low impedance of PEDOT:PSS on bacterial cellulose (BC) is related to the morphological structure of the BC membrane as shown in Fig. 4 (a). Bacterial cellulose is formed by an entangled mesh of nanofibers, approximately 100 nm thick and several microns long. Living cells seeded on these substrates encounter a 3D-like

surface, as schematically represented in Fig. 4 (b), that better mimics the extracellular matrix. Fig. 4 (c) shows an AFM topography image of the cellulose coated with a PEDOT:PSS thin film. The corresponding profile view is shown in Fig. 4 (d). The roughness of cellulose means it has valleys that can reach 180 nm deep. When the PEDOT:PSS ink impregnates the upper cellulose fibers, it enhances the active area of the electrode.

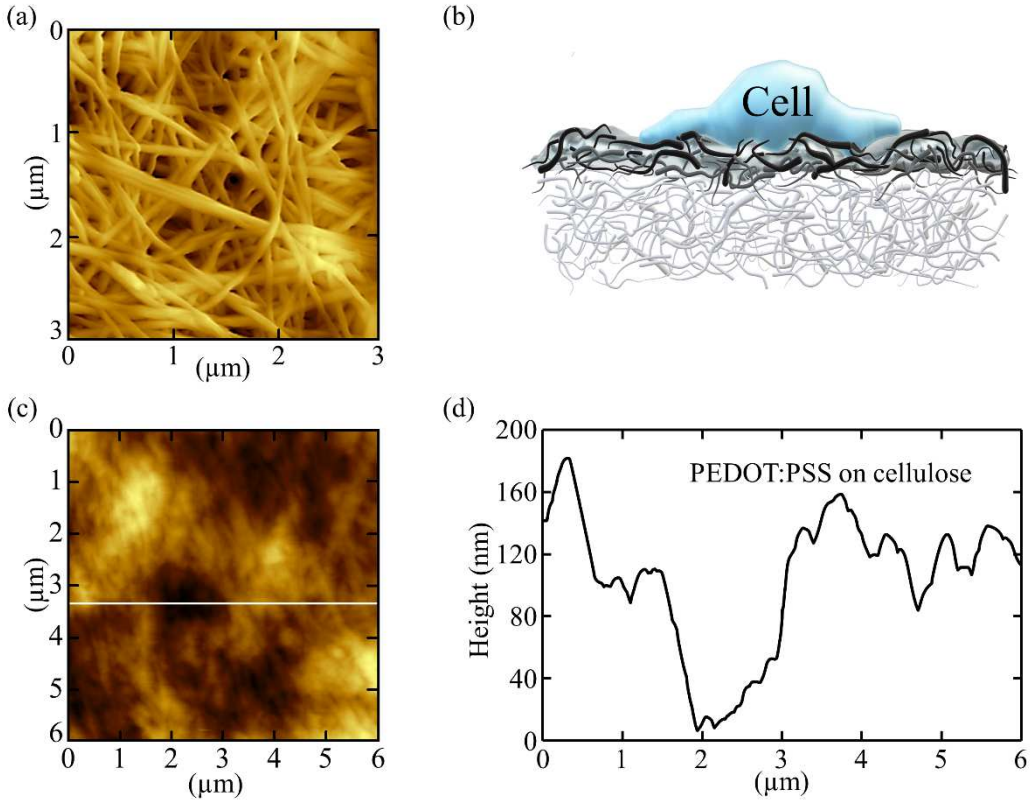

Fig. 4. Morphology of the bacterial cellulose substrate. (a) Topography AFM image with a scan area of 3x3 μm^2 of the surface of the bacterial cellulose showing nano-fibrillar structures. (b) Schematic representation of the PEDOT:PSS sensing electrode with cells on the bacterial cellulose substrate. (c) Topography AFM image of inkjet-printed PEDOT:PSS on bacterial cellulose**.** (d) Profile view of the PEDOT:PSS/bacterial cellulose electrode.

The frequency dependence of the noise (S_V) for the four types of electrodes under study is compared in Fig. 5. The amplifier noise ($S_V = 10^{-17}$ V^2/Hz for a bandwidth higher than 300 Hz) is well below the noise generated by the electrodes and all extrinsic noise sources have been minimized by appropriate shielding and grounding

as described in the experimental section. The gold electrode, deposited either on glass or on cellulose, has the highest noise. The higher noise of the gold electrode is in line with the higher interfacial resistance. The lowest thermal noise (S_V = 6 nV r.m.s) is observed for frequencies above 100 Hz and this noise is achieved when PEDOT:PSS is printed on bacterial cellulose, in agreement with the lowest interfacial resistance. The noise power spectral density analysis also shows that, for frequencies above 10 Hz, the noise of PEDOT:PSS on bacterial cellulose is one order of magnitude lower than the noise generated by a gold electrode on cellulose (Fig. 5).

The extremely low noise of the PEDOT:PSS-based electrodes extends up to frequencies as high as 100 kHz, also covering the frequency band used to measure action potentials. Although, this work has focused on the recording of low frequency signals, where noise is a critical issue, in reality PEDOT:PSS electrodes are advantageous over the full frequency range used to measure electrophysiological signals.

The pink noise ($1/f^2$ dependence) is common to all electrodes. With the exception of the curve corresponding to the PEDOT:PSS on glass, all the other curves shown in Fig. 5 run parallel to each other. This independence of the $1/f$ noise on the electrode material may shed some light into the physical origin of this type of noise in electrode/electrolyte systems.

The spectral dependence of the noise measured in current for a PEDOT:PSS-based electrode on a cellulose substrate is shown in the inset of Fig. 5. The noise in current shows two distinct spectral regions separated by a valley centered at 1 Hz. Below 1 Hz, the noise increases following the $1/f$ dependence. In contrast, above 1 Hz the noise increases until a plateau is reached at a frequency of 100 Hz. When measured in current detection method, the noise of the PEDOT:PSS electrode on cellulose has two relevant features; (i) it follows a $1/f$ dependency, which is a smoother rise than the $1/f^2$ dependence observed in voltage detection mode and, (ii) the onset of the $1/f$ tail begins one decade lower in frequency than the $1/f^2$ tail. These two aspects of the current detection mode are beneficial for low frequency measurements because they contribute to increase the SNR.

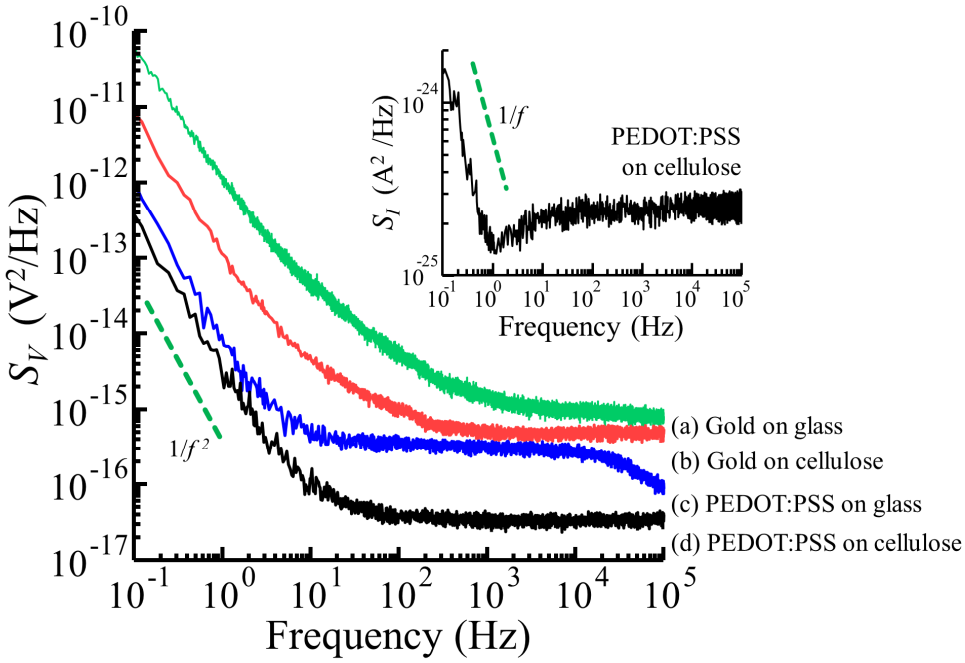

Fig. 5. Noise power spectral density (S_V) for the four different types of electrodes (gold and PEDOT:PSS, deposited on glass or on bacterial cellulose) evaluated in this study. (a)-magenta, gold on glass; (b)-red, gold on bacterial cellulose; (c)-blue, PEDOT:PSS on glass and (d)-black, PEDOT:PSS on cellulose. The inset shows the noise of the PEDOT:PSS on cellulose electrode when measured as current.

Having characterized the intrinsic noise of the electrodes, we now proceed to show how the noise affects the quality of the recorded signal. The best way to evaluate the relative performance of our sensing electrodes is to use a well-defined bioelectrical signal source and perform comparative recordings will all the electrodes. For this purpose, a surgically extracted zebrafish heart was placed on top of the sensing electrode. To assure that the signal strength was identical in all experiments, the same zebrafish heart was moved between devices and used for all the electrodes under study. This procedure was used as proof of concept, assuring that the signal strength was equal in all the experiments. The relative quality of the signals recorded by the different electrodes was compared and is shown in Fig. 6 (a) and (b). The highest SNR of 55 (in voltage detection mode) was obtained using PEDOT:PSS on bacterial cellulose and the poorest recordings (SNR=10) were obtained with a gold electrode on the cellulose substrate. As described above, the high signal quality obtained using

PEDOT:PSS on bacterial cellulose is due to the lower noise and to the higher interfacial capacitance. The relative values of the SNR are shown in the bar plot in Fig. 6 (c) for both voltage and current detection modes. The comparative effect of detecting signals in voltage or in current has been addressed in our previous works [26].

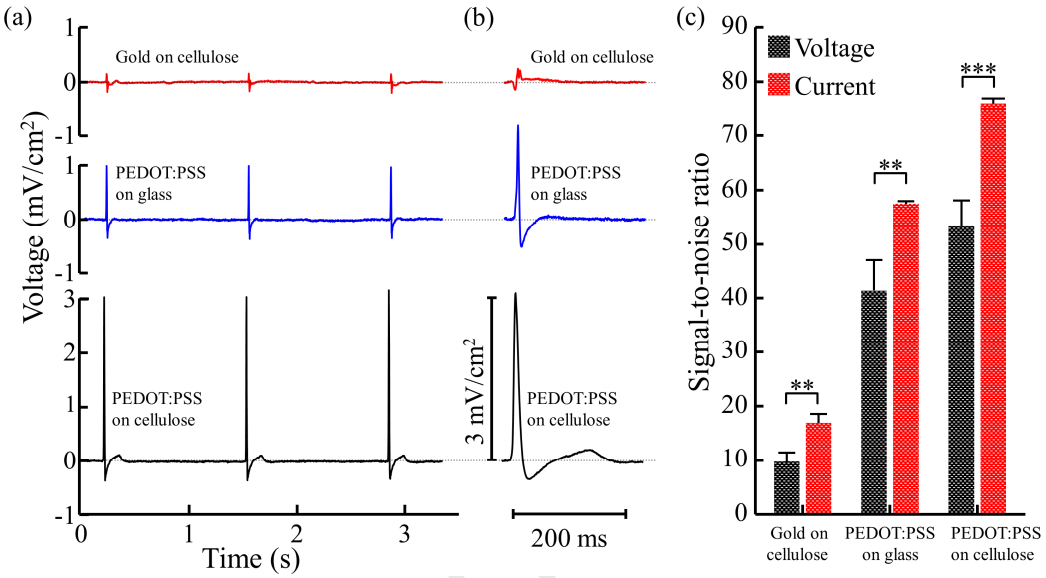

Fig. 6. Comparison of the signal quality obtained using diffent types of electrodes. (a)Three consecutive zebrafish heart beatings. (b) Detail view of individual signals. (c) Signal-to-noise ratio measured both in current and voltage detection mode in different types of electrodes. Signals were generated by placing the same zebrafish heart on top of each of the electrodes. ** and *** denote significant differences between SNR values detected in voltage and current modes of $p < 0.01$ and $p < 0.001$ (Student *t*-test), respectively.

3.2- Effect of the electrode/electrolyte interfacial resistance on the signal shape

The low interfacial resistance of the PEDOT:PSS/electrolyte interface minimizes the thermal noise and the recorded signal shape is such that improves the SNR. In order to understand the role of the resistance and capacitance in the definition of the signal shape, we need to analyze the current flowing through the equivalent circuit that describes the electrode/electrolyte interface, as shown in Fig. 7(a). In this analysis, the bulk electrolyte layer is described by the resistance R_E. In the equivalent circuit represented in Fig. 2 C_E was ignored because it is relatively small when compared with C_D. When a single square voltage pulse is applied to the device, the current i_S (t)

that flows through the system consists of two components, one is the displacement current through C_D, and the other is a steady state current flowing through R_D:

$$i_S(t) = C_D \frac{dv_C(t)}{dt} + \frac{v_C(t)}{R_D} \quad (1)$$

To calculate $i_s(t)$ the differential Eq. 1 for the voltage, $v_C(t)$, across the capacitor C_D has to be solved [46]. The analytical solution is given in terms of the time constant τ

$$\tau = \frac{R_D R_E C_D}{R_D + R_E} \quad (2)$$

τ in Eq. 2 is the time constant of an RC circuit with an effective resistance consisting of two in-parallel resistors (R_D and R_E).

To visualize how the circuit time constant affects the shape of the signal, an experiment was performed in which a well-defined square-like signal from a signal generator was applied to the counter electrode. The flow of signal through the EDL was recorded as current signal on the sensing electrode.

The signal shapes recorded in current upon the application of an input voltage pulse of 100 μV for 2 s is presented in Fig. 7 (b). When the signal was recorded with a gold electrode (see red curve on Fig 7 (b)), the corresponding signal in current was comprised of two current spikes, one upward at the rising edge and another downward at the falling edge of the voltage pulse, which are displacement currents. When the voltage was constant, the current fell rapidly to zero because the gold/electrolyte interface behaved almost as a purely capacitive interface. The application of an identical voltage pulse to a PEDOT:PSS-cellulose/electrolyte interface causes a slightly different response of the current signal, (see black curve in Fig 7 (b)).

The output current signal also contains the current displacement spikes, but now the current takes nearly 2 seconds to decay to a steady state. Fig. 7 (c) shows that the current decay is not a pure exponential as predicted by the simple equivalent circuit, but is comprised of a fast component (τ_1=0.25 s) followed by a slower component (τ_2=0.64 s). We will show that these times constants are one order of magnitude higher than the predicted time constant based on Eq. 2.

To obtain τ using Eq. 2 we need to know the quasi-static values of C_D, R_D and R_E. However both C_D and R_D are frequency dependent and the lowest frequency of our

impedance analyzer is 60 Hz. To obtain the quasi-static values we measured a series of current-voltage (*I-V*) loops with voltage ramps with a scanning speed of 20-30 mV/s (not shown). The voltage range was limited to only 100 mV to minimize charging effects and redox reactions. From the hysteresis in the *I-V* loops, we extract the displacement component that is related with the quasi-static capacitance, (C_D=100 μF) and from the DC component we extracted the quasi-static resistance (R_D=12.5 kΩ). The quasi-static capacitance is 134 times higher than the capacitance measured at 60 Hz (C_D=742 nF) and the quasi-static resistance is 10 times higher than the resistance measured at 60 Hz (R_D=1.2kΩ). Using the quasi-static impedance values in Eq. 2 we estimate a τ of 34 ms, a value that is one order of magnitude lower than the values of 250 ms or 640 ms experimentally recorded.

We propose that the slow response of the PEDOT:PSS/electrolyte interface upon the application of a voltage step is caused by a charging effect on the PEDOT:PSS electrode. The application of a voltage step on the PEDOT:PSS electrodes causes outflow or inflow (depending on the voltage sign) of ionic species at the PEDOT:PSS electrode, moving the interface out of equilibrium. At the outer interface with the electrolyte, ion diffusion occurs at on a fast time-scale; the non-equilibrium state generated by the voltage pulses is then rapidly re-equilibrated. However, ions that were pushed deeper into the PEDOT:PSS by the external field will face not only a constricted environment but also longer pathways to diffuse out to the free electrolyte. The consequence is that a longer time is needed for the system to re-attain again equilibrium once it has been displaced from it upon a voltage pulse. In summary, the shape of the current transient suggests that it is the redistribution of the ionic charges that governs the transient response time and not the RC time constant as estimated by simple equivalent circuit modeling. These results are in agreement with the reported transient response of organic electrochemical transistors, where it is claimed that the ion redistribution in the film determines the transient response [51],[52], and in neuromorphic devices [54]. For example, it is known that protons, (H^+), can easily be transported via the water molecules within the PEDOT PSS film through Grotthuss mechanism where protons will be transported from one water molecule to another through hydrogen bonding [53].

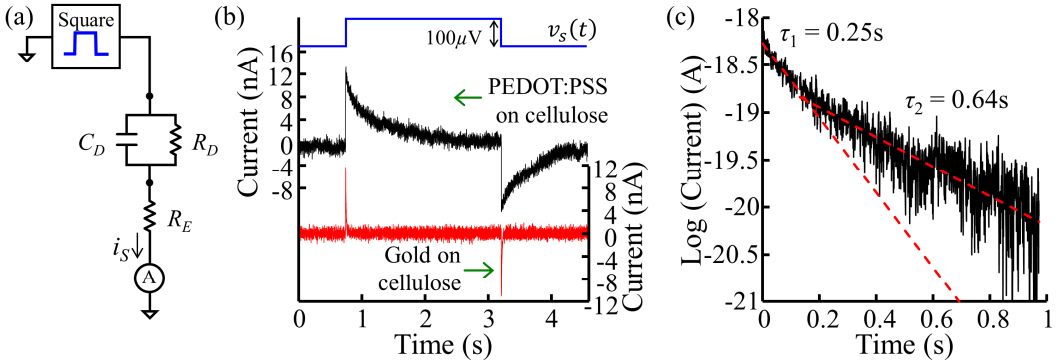

Fig. 7. The electrical signal recorded on different electrodes upon the application of a square voltage pulse. (a) Equivalent circuit used to interpret the transient response to a voltage pulse. (b) Comparison of the response of a gold-based electrode with the response of a PEDOT:PSS electrode printed on a bacterial cellulose substrate. (c) semi-logarithmic plot of the current decay across the PEDOT/electrolyte interface on cellulose after the application of a voltage step of 100 µV. The dashed lines are fits to the fast (τ_1=0.25s) and slow decay components (τ_2=0.64 s).

3.3 Detection of signals in non-electrogenic cell populations

The optimized ultra-low noise PEDOT:PSS/bacterial cellulose electrodes were used to measure electrical fluctuations generated by populations of C6 glioma cells. Glioma cells synchronize their activity to generate cooperative oscillations. These oscillations travel across the cell network at speeds of 10-30 µm/s and often become quasi-periodic. Details about this bioelectrical phenomenon have previously been reported [30,55–58]. When the travelling oscillation hits the electrode, cells on top of the electrode synchronize and generate a voltage signal proportional to the width of the sensing electrode. Glioma cells are a robust model to evaluate the detection limits and the performance of our PEDOT:PSS-based electrodes. This is because glioma cells generate long-lasting signals fitting well in the class of signals generated by non-electrogenic cells, for instance astrocytes [25,31] and prostate cancer cells [29].

A time-trace in current of quasi-periodic bursts of activity of C6 glioma cells is shown in Fig. 8 (a). The pattern of activity is described in four spans: (i) silent region (green color); (ii) quasi-periodic signals, representing early synchronization of C6 cells (blue color); (iii) synchronized activity of C6 cells (black color); and (iv) weak and unsynchronized activity (red color). To identify the major signal frequencies, the inter-spike time intervals were analyzed and distributed into corresponding frequency

bins to build the histogram in Fig. 8 (b). This procedure was adopted because the signals were not periodic and had a broad distribution in frequency. For clarity, the bins on the histogram were distributed in a logarithmic frequency scale with 5 bins per interval of 10. The histogram shows that the dominant signal frequency is 0.126 ± 0.011 Hz.

A detailed view of 3 consecutive individual signals, measured both as a current and voltage signal is shown in Fig. 8 (c). The signal in voltage has a square-like shape of about 60 μV in amplitude and lasted for 2 seconds with an approximately 8 seconds periodicity and the corresponding signal in current followed the trend presented above. Displacement current spikes dominated the recorded signal edges. When the bioelectrical signal was measured as a current, both displacement currents and the dc contribution added together to strengthen the recorded bioelectrical signal.

To illustrate the dramatic effect of the electrode material on real recorded bioelectrical signals, three signals recorded for glioma cells are shown in Fig. 8 (d). In gold-based electrodes, the displacement spikes dominate the signal. In PEDOT:PSS based electrodes, the slow relaxing component becomes pronounced and the overall power of the signal is higher. As a consequence, there is a striking difference between the signal quality measured using bacterial cellulose and the other types of electrodes. The signals recorded using PEDOT:PSS/bacterial cellulose electrodes reach a SNR of 140, while SNR is only 89 for PEDOT:PSS on glass. The improvement in signal quality, is due, to the high capacitance, to a lower noise, and also to a charging effect on the PEDOT:PSS.

It is important to emphasize, that in addition to the minimization of the thermal noise, charging effects on the PEDOT:PSS are also crucial in re-shaping the measured bioelectrical signal and in improving the SNR. As shown in Fig. 7 (b), the slow decay in current upon the application of a voltage pulse, introduces a slow component, which we attribute to a charge redistribution within the polymer. This charging effect should also occur in the PEDOT:PSS, when exposed to small ionic fluctuations generated by the cells. Fig. 8 (c) shows clearly that the biosignal in voltage has a square-like component. This shape is expected because the native biosignal is a traveling wave crossing an electrode of a defined width as described in our previous publication [57]. However, the square voltage shape is followed by a slow component with a τ between 1.2 and 1.5 s. This slow relaxing phenomenon is in agreement with

our previous analysis carried out using the simulated signal described in Fig.7. It is plausible that this slow decay of the biosignal is due to charges slowly relaxing back to equilibrium after oscillation has passed trough the electrode.

The voltage signal generated by the cell population may not be a symmetric signal, which means that the amplitude of the rising edge is not necessarily equal to the amplitude of the falling edge. This asymmetry becomes more pronounced when the signal is measured in current, because the displacement spike is proportional to d*v*/d*t* as shown in Eq.1. This feature may explain why the signal recorded using the gold electrode (in Fig 8 (d)) is strongly asymmetric.

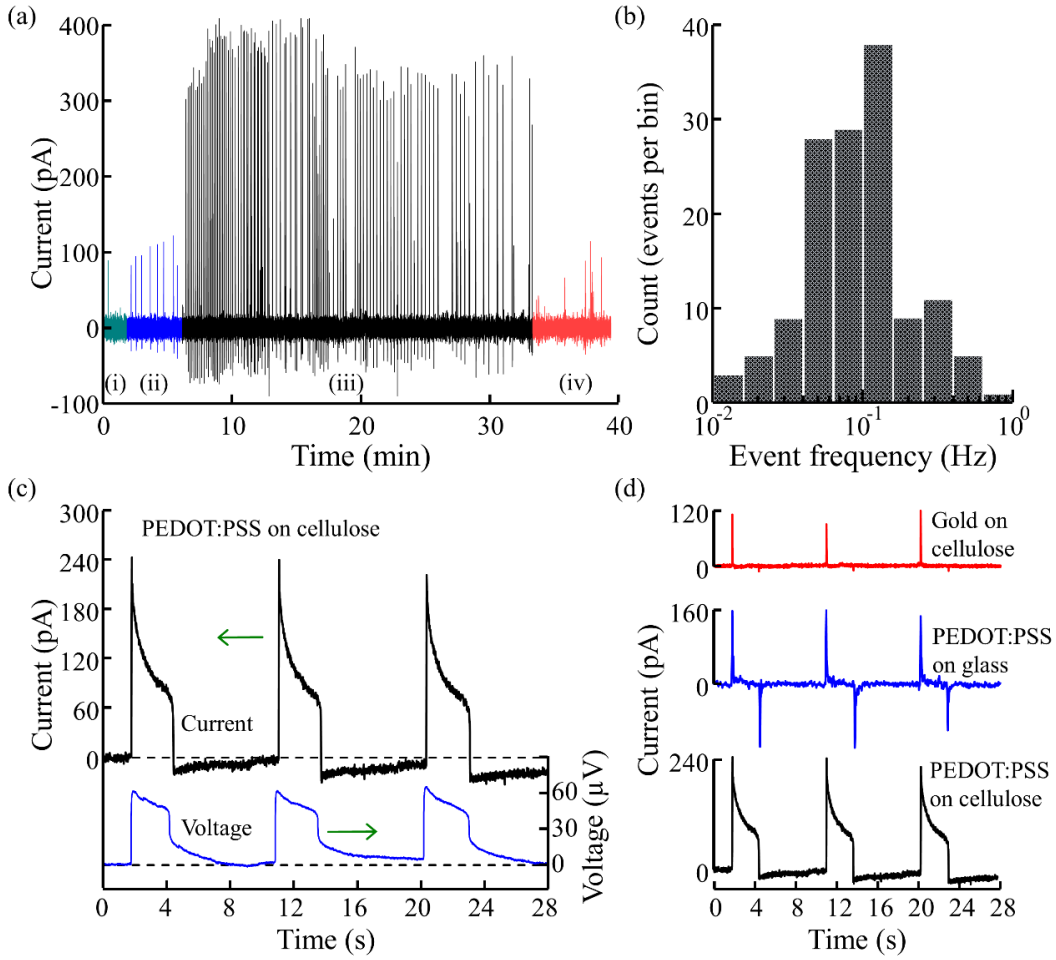

Fig. 8. (a) Time trace of current signals recorded in glioma cells using PEDOT:PSS-based electrodes in BC. (b) Histogram of the number of signals distributed into frequency slots. (c) Detailed view of the voltage and current signals recorded from a glioma population using a PEDOT:PSS/bacterial cellulose electrode. (d) Comparison of the signals recorded from a glioma cell population using different types of electrodes.

4- Discussion and conclusions

PEDOT:PSS/electrolyte interface has a very low intrinsic thermal noise in the frequency range from 0.1 Hz up to 100 kHz. In this frequency range, the noise of the PEDOT:PSS electrode is one order of magnitude lower than that noise generated by the gold electrode. The low intrinsic thermal noise maximizes the SNR ratio and makes the PEDOT:PSS-based electrodes ideally suited to measure a variety of electrophysiological signals, including action potentials and long lasting oscillations generated by non-excitable cells.

In comparison with flat hard substrates, the use of bacterial cellulose as substrate lowers the PEDOT:PSS impedance. The findings reported here suggest that the cellulose fibrous structure creates a micro-porosity that enhances the effective area of the electrical double-layers formed between the two phases of the PEDOT:PSS, the nano-scale PEDOT-rich and PSS-rich interconnected grains. Therefore, bacterial cellulose substrate takes full advantage of the electronic properties related with two-phase structure of PEDOT:PSS.

Moreover, we showed the influence of PEDOT:PSS charging effects on shaping the biosignal decay. We demonstrated that, when the signals are long lasting (a few seconds long), the slow relaxation of the charge distribution to equilibrium state contributes to enhance the SNR.

Because noise is critical at low frequencies, this study is focused on the electrode requirements that must be satisfied to record low-frequency signals from non-electrogenic cells. The interfacial resistance between the electrode and the electrolyte solution plays a crucial role because it controls the intrinsic noise generated by the electrode and also the long relaxation time to a steady component that influences the recorded signal shape. Using electrodes based on PEDOT:PSS deposited on glass and on bacterial cellulose substrates, we experimentally evaluated the electrode performance in the recording of extracellular action potentials from zebrafish hearts and ultra-slow (0.1 Hz) oscillations from glioma cell populations.

To detect long lasting signals, the bottleneck that determines the detection limit is the $1/f^2$ noise. Here, we show that the low EDL resistance of the PEDOT:PSS printed on bacterial cellulose provides a way to minimize the deleterious effects of the $1/f^2$ noise. These findings should be of value in configuring *in vitro* and *in vivo* extracellular electrode arrays for recording non-electrogenic cells in various applications.

Particularly interesting research fields are astrocyte-neuron communications [59–61] and cancer research [27,62,63]. In addition to the advantage of low intrinsic thermal noise, bacterial cellulose substrates are soft, biocompatible and low cost. Furthermore, bacterial cellulose-based electrodes do not represent a future environmental hazard.

Acknowledgments

We gratefully acknowledge support from the Portuguese Foundation for Science and Technology (FCT/MCTES), through national funds and when applicable co-funded EU funds by FEDER under the PT 2020 Partnership Agreement.

The projects contributing to this work are the following ones: PTDC/EEIAUT/5442/2014 (“Implantable organic devices for advanced therapies”, INNOVATE), UID/EEA/50008/2020 (Instituto de Telecomunicações, IT), UID/Multi/04326/2020 (Centro de Ciências do Mar, CCMar), and CICECO – Aveiro Institute of Materials (UIDB/50011/2020 & UIDP/50011/2020). RCF was funded by FCT, under the “Norma Transitória” -DL57/2016/CP1361/ project CT0020 and AM was funded by an FCT PhD grant SFRH/BD/148688/2019.

References

1. Zeglio, E.; Rutz, A.L.; Winkler, T.E.; Malliaras, G.G.; Herland, A. Conjugated Polymers for Assessing and Controlling Biological Functions. *Adv. Mater.* **2019**, *31*, 1806712.
2. Aqrawe, Z.; Montgomery, J.; Travas-Sejdic, J.; Svirskis, D. Conducting Polymers as Electrode Coatings for Neuronal Multi-electrode Arrays. *Trends Biotechnol.* **2017**, *35*, 93–95.
3. Garma, L.D.; Ferrari, L.M.; Scognamiglio, P.; Greco, F.; Santoro, F. Inkjet-printed PEDOT:PSS multi-electrode arrays for low-cost: In vitro electrophysiology. *Lab Chip* **2019**, *19*, 3776–3786.
4. Rivnay, J.; Owens, R.M.; Malliaras, G.G. The rise of organic bioelectronics. *Chem. Mater.* **2014**, *26*, 679–685.
5. Di Lauro, M.; Benaglia, S.; Berto, M.; Bortolotti, C.A.; Zoli, M.; Biscarini, F. Exploiting interfacial phenomena in organic bioelectronics: Conformable devices for bidirectional communication with living systems. *Colloids Surfaces B Biointerfaces* **2018**, *168*, 143–147.
6. Koutsouras, D.A.; Hama, A.; Pas, J.; Gkoupidenis, P.; Supérieure, E.N. PEDOT : PSS microelectrode arrays for hippocampal cell culture electrophysiological recordings. **2018**, *7*, 259–265.
7. Sessolo, M.; Khodagholy, D.; Rivnay, J.; Maddalena, F.; Gleyzes, M.; Steidl, E.; Buisson, B.; Malliaras, G.G. Easy-to-Fabricate Conducting Polymer Microelectrode Arrays. *Adv. Mater.* **2013**, *25*, 2135–2139.
8. Green, R.A.; Lovell, N.H.; Wallace, G.G.; Poole-Warren, L.A. Conducting polymers for neural interfaces: Challenges in developing an effective long-term implant. *Biomaterials* **2008**, *29*, 3393–3399.
9. Inal, S.; Rivnay, J.; Suiu, A.-O.; Malliaras, G.G.; McCulloch, I. Conjugated Polymers in Bioelectronics. *Acc. Chem. Res.* **2018**, *51*, 1368–1376.
10. Berggren, M.; Richter-Dahlfors, A. Organic Bioelectronics. *Adv. Mater.* **2007**, *19*, 3201–3213.
11. Hempel, F.; Law, J.K.; Chien, T.; Munief, W.; Lu, X. Biosensors and Bioelectronics PEDOT : PSS organic electrochemical transistor arrays for extracellular electrophysiological sensing of cardiac cells. *Biosens. Bioelectron.* **2017**, *93*, 132–138.
12. Jonsson, A.; Inal, S.; Uguz, I.; Williamson, A.J.; Kergoat, L.; Rivnay, J.; Khodagholy, D.; Berggren, M.; Bernard, C.; Malliaras, G.G.; Simon, D.T.. Bioelectronic neural pixel : Chemical stimulation and electrical sensing at the same site. **2016**, *113*, *9440-9445*.
13. Nyberg, T.; Shimada, A.; Torimitsu, K. Ion conducting polymer microelectrodes for interfacing with neural networks. *J. Neurosci. Methods* **2007**, *160*, 16–25.
14. Bihar, E.; Roberts, T.; Saadaoui, M.; Hervé, T.; De Graaf, J.B.; Malliaras, G.G. Inkjet-Printed PEDOT:PSS Electrodes on Paper for Electrocardiography. *Adv. Healthc. Mater.* **2017**, *6*, 1601167.
15. Inacio, P.M.C.; Mestre, A.L.G.; De Medeiros, M.D.C.R.; Asgarifar, S.; Elamine, Y.; Canudo, J.; Santos, J.M.A.; Bragança, J.; Morgado, J.; Biscarini, F.; et al. Bioelectrical Signal Detection Using Conducting Polymer Electrodes and the Displacement Current Method. *IEEE Sens. J.* **2017**, *17*, 3961–3966.
16. Spira, M.E.; Hai, A. Multi-electrode array technologies for neuroscience and cardiology. *Nat. Nanotechnol.* **2013**, *8*, 83–94.

17. Ganji, M.; Kaestner, E.; Hermiz, J.; Rogers, N.; Tanaka, A.; Cleary, D.; Lee, S.H.; Snider, J.; Halgren, M.; Cosgrove, G.R.; et al. Development and Translation of PEDOT:PSS Microelectrodes for Intraoperative Monitoring. *Adv. Funct. Mater.* **2018**, *28*, 1700232
18. Qi, D.; Liu, Z.; Liu, Y.; Jiang, Y.; Leow, W.R.; Pal, M.; Pan, S.; Yang, H.; Wang, Y.; Zhang, X.; et al. Highly Stretchable, Compliant, Polymeric Microelectrode Arrays for In Vivo Electrophysiological Interfacing. *Adv. Mater.* **2017**, *29*, 1–10.
19. Rivnay, J.; Leleux, P.; Ferro, M.; Sessolo, M.; Williamson, A.; Koutsouras, D.A.; Khodagholy, D.; Ramuz, M.; Strakosas, X.; Owens, R.M.; et al. High-performance transistors for bioelectronics through tuning of channel thickness. *Sci. Adv.* **2015**, *1*, 1–6.
20. Proctor, C.M.; Rivnay, J.; Malliaras, G.G. Understanding volumetric capacitance in conducting polymers. *J. Polym. Sci. Part B Polym. Phys.* **2016**, *54*, 1433–1436.
21. Volkov, A. V.; Wijeratne, K.; Mitraka, E.; Ail, U.; Zhao, D.; Tybrandt, K.; Andreasen, J.W.; Berggren, M.; Crispin, X.; Zozoulenko, I. V. Understanding the Capacitance of PEDOT:PSS. *Adv. Funct. Mater.* **2017**, *27*, 1700329.
22. Milotti, E. 1/F Noise: a Pedagogical Review. **2002**.
23. Parkash, J.; Asotra, K. Calcium wave signaling in cancer cells. *Life Sci.* **2010**, *87*, 587–595.
24. Kolch, W.; Halasz, M.; Granovskaya, M.; Kholodenko, B.N. The dynamic control of signal transduction networks in cancer cells. *Nat. Publ. Gr.* **2015**, *15*, 515–527.
25. Mestre, A.L.G.; Cerquido, M.; Inácio, P.M.C.; Asgarifar, S.; Lourenço, A.S.; Cristiano, M.L.S.; Aguiar, P.; Medeiros, M.C.R.; Araújo, I.M.; Ventura, J.; et al. Ultrasensitive gold micro-structured electrodes enabling the detection of extra-cellular long-lasting potentials in astrocytes populations. *Sci. Rep.* **2017**, *7*, 14284.
26. Mestre, A.L.G.; Inácio, P.M.C.; Elamine, Y.; Asgarifar, S.; Lourenço, A.S.; Cristiano, M.L.S.; Aguiar, P.; Medeiros, M.C.R.; Araújo, I.M.; Ventura, J.; et al. Extracellular Electrophysiological Measurements of Cooperative Signals in Astrocytes Populations. *Front. Neural Circuits* **2017**, *11*, 1–9.
27. Rocha, P.R.F.; Medeiros, M.C.R.; Kintzel, U.; Vogt, J.; Araújo, I.M.; Mestre, A.L.G.; Mailänder, V.; Schlett, P.; Dröge, M.; Schneider, L.; et al. Extracellular electrical recording of pH-triggered bursts in C6 glioma cell populations. *Sci. Adv.* **2016**, *2*, e1600516.
28. Asgarifar, S.; Mestre, A.L.G.; Félix, R.C.; Inácio, P.M.C.; Cristiano, M.L.S.; Medeiros, M.C.R.; Araújo, I.M.; Power, D.M.; Gomes, H.L. Extracellular electrophysiological based sensor to monitor cancer cells cooperative migration and cell-cell connections. *Biosens. Bioelectron.* **2019**, *145*, 111708.
29. Cabello, M.; Ge, H.; Aracil, C.; Moschou, D.; Estrela, P.; Quero, J.M.; Pascu, S.I.; Rocha, P.R.F. Extracellular electrophysiology in the prostate cancer cell model PC-3. *Sensors (Switzerland)* **2019**, *19*, 1–11.
30. Borrachero-Conejo, A.I.; Saracino, E.; Natali, M.; Prescimone, F.; Karges, S.; Bonetti, S.; Nicchia, G.P.; Formaggio, F.; Caprini, M.; Zamboni, R.; et al. Electrical Stimulation by an Organic Transistor Architecture Induces Calcium Signaling in Nonexcitable Brain Cells. *Adv. Healthc. Mater.* **2019**, *8*, 1–12.
31. Saracino, E.; Maiolo, L.; Polese, D.; Semprini, M.; Borrachero-Conejo, A.I.; Gasparetto, J.; Murtagh, S.; Sola, M.; Tomasi, L.; Valle, F.; et al. A Glial-

Silicon Nanowire Electrode Junction Enabling Differentiation and Noninvasive Recording of Slow Oscillations from Primary Astrocytes. *Adv. Biosyst.* **2020**, *1900264*, 1900264.

32. Klemm, D.; Cranston, E.D.; Fischer, D.; Gama, M.; Kedzior, S.A.; Kralisch, D.; Kramer, F.; Kondo, T.; Lindström, T.; Nietzsche, S.; et al. Nanocellulose as a natural source for groundbreaking applications in materials science: Today's state. *Mater. Today* **2018**, *21*, 720–748.
33. Rambo, C.R.; Recouvreux, D.O.S.; Carminatti, C.A.; Pitlovanciv, A.K.; Antônio, R. V.; Porto, L.M. Template assisted synthesis of porous nanofibrous cellulose membranes for tissue engineering. *Mater. Sci. Eng. C* **2008**, *28*, 549–554.
34. Petersen, N.; Gatenholm, P. Bacterial cellulose-based materials and medical devices: current state and perspectives. *Appl. Microbiol. Biotechnol.* **2011**, *91*, 1277–1286.
35. Lv, X.; Yang, J.; Feng, C.; Li, Z.; Chen, S.; Xie, M.; Huang, J.; Li, H.; Wang, H.; Xu, Y. Bacterial Cellulose-Based Biomimetic Nanofibrous Scaffold with Muscle Cells for Hollow Organ Tissue Engineering. *ACS Biomater. Sci. Eng.* **2015**, *2*, 19–29.
36. Meftahi, A.; Nasrolahi, D.; Babaeipour, V.; Alibakhshi, S.; Shahbazi, S. Investigation of Nano Bacterial Cellulose Coated by Sesamum Oil for Wound Dressing Application. *Procedia Mater. Sci.* **2015**, *11*, 212–216.
37. Kim, J.; Kim, S.W.; Park, S.; Lim, K.T.; Seonwoo, H.; Kim, Y.; Hong, B.H.; Choung, Y.H.; Chung, J.H. Bacterial cellulose nanofibrillar patch as a wound healing platform of tympanic membrane perforation. *Adv. Healthc. Mater.* **2013**, *2*, 1525–1531.
38. Silvestre, A.J.D.; Freire, C.S.R.; Neto, C.P. Do bacterial cellulose membranes have potential in drug-delivery systems? *Expert Opin. Drug Deliv.* **2014**, *11*, 1113–24.
39. Silva, N.H.C.S.; Drumond, I.; Almeida, I.F.; Costa, P.; Rosado, C.F.; Neto, C.P.; Freire, C.S.R.; Silvestre, A.J.D. Topical caffeine delivery using biocellulose membranes: a potential innovative system for cellulite treatment. *Cellulose* **2013**, *21*, 665–674.
40. Trovatti, E.; Freire, C.S.R.; Pinto, P.C.; Almeida, I.F.; Costa, P.; Silvestre, A.J.D.; Neto, C.P.; Rosado, C. Bacterial cellulose membranes applied in topical and transdermal delivery of lidocaine hydrochloride and ibuprofen: In vitro diffusion studies. *Int. J. Pharm.* **2012**, *435*, 83–87.
41. Almeida, I.F.; Pereira, T.; Silva, N.H.C.S.; Gomes, F.P.; Silvestre, A.J.D.; Freire, C.S.R.; Sousa Lobo, J.M.; Costa, P.C. Bacterial cellulose membranes as drug delivery systems: An in vivo skin compatibility study. *Eur. J. Pharm. Biopharm.* **2014**, *86*, 332–336.
42. Carvalho, T.; Guedes, G.; Sousa, F.L.; Freire, C.S.R.; Santos, H.A. Latest Advances on Bacterial Cellulose-Based Materials for Wound Healing, Delivery Systems, and Tissue Engineering. *Biotechnol. J.* **2019**, *14*, 1–19.
43. Silva, N.H.C.S.; Mota, J.P.; de Almeida, T.S.; Carvalho, J.P.F.; Silvestre, A.J.D.; Vilela, C.; Rosado, C.; Freire, C.S.R. Topical drug delivery systems based on bacterial nanocellulose: Accelerated stability testing. *Int. J. Mol. Sci.* **2020**, *21*, 1262.
44. Trovatti, E.; Serafim, L.S.; Freire, C.S.R.; Silvestre, A.J.D.; Neto, C.P. Gluconacetobacter sacchari: An efficient bacterial cellulose cell-factory. *Carbohydr. Polym.* **2011**, *86*, 1417–1420.

45. Bagheri, A.; Salam, M.T.; Velazquez, J.L.P.; Genov, R. Low-Frequency Noise and Offset Rejection in DC-Coupled Neural Amplifiers: A Review and Digitally-Assisted Design Tutorial. *IEEE Trans. Biomed. Circuits Syst.* **2017**, *11*, 161–176.
46. Medeiros, M.C.R.; Mestre, A.; Inácio, P.; Asgarif, S.; Araújo, I.M.; Hubbard, P.C.; Velez, Z.; Cancela, M.L.; Rocha, P.R.F.; de Leeuw, D.M.; et al. An electrical method to measure low-frequency collective and synchronized cell activity using extracellular electrodes. *Sens. Bio-Sensing Res.* **2016**, *10*, 1–8.
47. Brittinger, M.; Fromherz, P. Field-effect transistor with recombinant potassium channels: Fast and slow response by electrical and chemical interactions. *Appl. Phys. A Mater. Sci. Process.* **2005**, *81*, 439–447.
48. Rocha, P.R.F.F.; Schlett, P.; Kintzel, U.; Mailänder, V.; Vandamme, L.K.J.J.; Zeck, G.; Gomes, H.L.; Biscarini, F.; de Leeuw, D.M. Electrochemical noise and impedance of Au electrode/electrolyte interfaces enabling extracellular detection of glioma cell populations. *Sci. Rep.* **2016**, *6*, 34843.
49. Massobrio, G.; Martinoia, S.; Massobrio, P. Equivalent Circuit of the Neuro-Electronic Junction for Signal Recordings From Planar and Engulfed Micro-Nano-Electrodes. *IEEE Trans. Biomed. Circuits Syst.* **2017**, 1–10.
50. Jing Guo; Jie Yuan; Mansun Chan Modeling of the Cell-Electrode Interface Noise for Microelectrode Arrays. *IEEE Trans. Biomed. Circuits Syst.* **2012**, *6*, 605–613.
51. Franks, W.; Schenker, I.; Schmutz, P.; Hierlemann, A. Impedance Characterization and Modeling of Electrodes for Biomedical Applications. *IEEE Trans. Biomed. Eng.* **2005**, *52*, 1295–1302.
52. Hassibi, A.; Navid, R.; Dutton, R.W.; Lee, T.H. Comprehensive study of noise processes in electrode electrolyte interfaces. *J. Appl. Phys.* **2004**, *96*, 1074–1082.
53. Viswam, V.; Obien, M.E.J.; Franke, F.; Frey, U.; Hierlemann, A. Optimal electrode size for multi-scale extracellular-potential recording from neuronal assemblies. *Front. Neurosci.* **2019**, *13*, 1–23.
54. Giordani, M.; Sensi, M.; Berto, M.; Di Lauro, M.; Bortolotti, C.A.; Gomes, H.L.; Zoli, M.; Zerbetto, F.; Fadiga, L.; Biscarini, F. Neuromorphic Organic Devices that Specifically Discriminate Dopamine from Its Metabolites by Nonspecific Interactions. *Adv. Funct. Mater.* **2020**, *2002141*, 1–13.
55. Asgarifar, S.; Inácio, P.M.C.; Mestre, A.L.G.; Gomes, H.L. Ultrasensitive bioelectronic devices based on conducting polymers for electrophysiology studies. *Chem. Pap.* **2018**, *72*, 1597–1603.
56. Charles, A.C.; Naus, C.C.; Zhu, D.; Kidder, G.M.; Dirksen, E.R.; Sanderson, M.J. Intercellular calcium signaling via gap junctions in glioma cells. *J. Cell Biol.* **1992**, *118*, 195–201.
57. Kuga, N.; Sasaki, T.; Takahara, Y.; Matsuki, N.; Ikegaya, Y. Large-Scale Calcium Waves Traveling through Astrocytic Networks In Vivo. *J. Neurosci.* **2011**, *31*, 2607–2614.
58. Verkhratsky, A.; Orkand, R.K.; Kettenmann, H. Glial calcium: homeostasis and signaling function. *Physiol. Rev.* **1998**, *78*, 99–141.
59. Adams, D.S.; Levin, M. Endogenous voltage gradients as mediators of cell-cell communication: strategies for investigating bioelectrical signals during pattern formation. *Cell Tissue Res.* **2013**, *352*, 95–122.
60. Balaji, R.; Bielmeier, C.; Harz, H.; Bates, J.; Stadler, C.; Hildebrand, A.; Classen, A.-K. Calcium spikes, waves and oscillations in a large, patterned

epithelial tissue. *Sci. Rep.* **2017**, *7*, 42786.
61. Volterra, A.; Meldolesi, J. Astrocytes, from brain glue to communication elements: the revolution continues. *Nat. Rev. Neurosci.* **2005**, *6*, 626–640.
62. Jung, E.; Alfonso, J.; Osswald, M.; Monyer, H.; Wick, W.; Winkler, F. Emerging intersections between neuroscience and glioma biology. *Nat. Neurosci.* **2019**, *22*, 1951–1960.
63. Maklad, A.; Sharma, A.; Azimi, I. Calcium signaling in brain cancers: Roles and therapeutic targeting. *Cancers (Basel).* **2019**, *11*, 145.

Highlights:

- PEDOT:PSS-based electrodes in low frequency electrophysiology studies.
- PEDOT:PSS/electrolyte interfaces have a very low intrinsic noise.
- Charging effects on PEDOT:PSS electrodes improve the SNR in biosignal recordings.
- PEDOT:PSS-based electrodes provide access to signals in non-electrogenic cells.